

Density and correlation functions of vortex and saddle points in open billiard systems

R. Höhmann, U. Kuhl, and H.-J. Stöckmann

Fachbereich Physik der Philipps-Universität Marburg, Renthof 5, D-35032 Marburg, Germany

J. D. Urbina

*Department of Physics, Universidad Nacional de Colombia, Ciudad Universitaria, Bogota, Colombia
and Department of Physics, Regensburg Universität, 93047, Regensburg, Germany*

M. R. Dennis

H H Wills Physics Laboratory, University of Bristol, Tyndall Avenue, Bristol BS8 1TL, United Kingdom

(Received 21 August 2008; revised manuscript received 31 October 2008; published 15 January 2009)

We present microwave measurements for the density and spatial correlation of current critical points in an open billiard system and compare them with new and previous predictions of the random-wave model (RWM). In particular, due to an improvement of the experimental setup, we determine experimentally the spatial correlation of saddle points of the current field. An asymptotic expression for the vortex-saddle and saddle-saddle correlation functions based on the RWM is derived, with experiment and theory agreeing well. We also derive an expression for the density of saddle points in the presence of a straight boundary with general mixed boundary conditions in the RWM and compare with experimental measurements of the vortex and saddle density in the vicinity of a straight wall satisfying Dirichlet conditions.

DOI: [10.1103/PhysRevE.79.016203](https://doi.org/10.1103/PhysRevE.79.016203)

PACS number(s): 05.45.Mt, 42.25.Bs

I. INTRODUCTION

The use of Gaussian random functions to describe the spatial structure of complex physical systems has had success in a wide range of physical applications, originating from Rice's description of the random currents of shot noise [1] and Longuet-Higgins' description of random water waves [2,3], and more recently in such diverse fields as sound waves and acoustics [4,5], turbulence [6], optical speckle patterns [7], and cosmic microwave background fluctuations [8].

In the realm of quantum-wave physics, the same universality of the amplitude fluctuations has been conjectured in the spatial patterns of eigenfunctions in systems with classical (ray) chaotic dynamics [9]. The analogy between the equations of a noninteracting two-dimensional electron gas and the electromagnetic modes of a microwave cavity [10–14] (see Refs. [15,16] for reviews) allows a unified treatment in the language of quantum billiards: namely, as solutions of the two-dimensional Helmholtz equation

$$-(\partial_x^2 + \partial_y^2)\psi(\vec{r}) = k^2\psi(\vec{r}), \quad (1)$$

with wave number k and energy k^2 , where $\vec{r}=(x,y)$. We therefore may study the properties of electron wave functions, which are otherwise difficult to access experimentally, by means of measurements using our microwave experimental setup. Previously, insights from this analogy have had a strong impact on the theoretical study of coherent effects on electronic systems in the mesoscopic regime, where the spatial correlations of the electronic wave function are, besides the fluctuations of the energy spectra, the source of mesoscopic reproducible fluctuations (see Refs. [17–19] for recent examples).

Concerning fundamental questions, the measurements of complicated statistical measures (namely, averages over the

experimentally constructed eigenfunctions of complicated functionals) are very stringent probes for the statistical assumptions upon which theoretical models of chaotic wave functions are based. The primary such model is the so-called random-wave model (RWM), proposed by Berry [9], based on the isotropic two-dimensional random waves studied by Longuet-Higgins [3]. The RWM we consider here is a statistically stationary isotropic solution of the two-dimensional Helmholtz equation (time-independent Schrödinger equation), statistically invariant to translation and rotation.

The RWM predicts that the spatial fluctuations of eigenfunctions are Gaussian distributed, and this gives rise to characteristic morphological features (e.g., Refs. [20,21]). So far, and largely due to the experimental possibility given by the microwave measurements, the assumption of Gaussian statistics has successfully passed very demanding tests. To mention just two examples where very complicated functionals of the measured eigenfunctions are required and the RWM provide excellent results, we have the distribution of current [22], the intensity distribution in the transition from closed to open billiards [23], and the distribution of quantum stress tensor [24] (see Ref. [16] for a recent review).

In this paper we address a different type of functional, based on the nodal properties of complex chaotic wave functions, and show again how the assumption of Gaussian statistics is strongly supported by the experimental results.

The features of the random eigenfunctions, we study here are the critical points of the current density (hereafter current) associated with the complex wave ψ . The current is defined by

$$\vec{j}(\vec{r}) \equiv \text{Im} \psi(\vec{r})^* \nabla \psi(\vec{r}). \quad (2)$$

In quantum-mechanical systems, $\vec{j}(\vec{r})$ represents the probability current density at position \vec{r} . In quasi-two-dimensional

electromagnetic microwave billiards, there is a one-to-one correspondence of $\vec{j}(\vec{r})$ to the Poynting vector [22].

Since ψ is assumed to satisfy the two-dimensional Helmholtz equation, the points where $\vec{j}=\vec{0}$ are of two types: vortices of the flow (also known as circulations, wave dislocations, nodal points, and phase singularities [16,22,25–27]), where $\psi=0$ and about which the current swirls in a counterclockwise (+) or clockwise (–) sense, and saddle points (stagnation points), which are also saddle points of the phase $\arg \psi$ and hyperbolic points in the current flow. (The existence of phase extrema—maxima or minima—is prohibited by the Helmholtz equation [27].) The topological Poincaré index of these types of points, describing the number of turns of \vec{j} in a small circuit of the critical point, is +1 for vortices (regardless of the sense of circulation) and –1 for saddle points. General arguments based on statistical isotropy demonstrate that there can be no net accumulation of topological charge, either in the sign of the vortices or in the Poincaré index. Therefore, the densities of positive and negative vortices must be equal, and the bulk vortex density must equal the bulk saddle density; calculations based on the RWM [25–27] give this vortex density as $k^2/4\pi$. Knowledge of the positions of the critical points of the current vector field provides a skeleton on which the rest of the flow field is based.

An important deviation to the bulk RWM is caused by the presence of boundaries. The interplay between spatial confinement and Gaussian fluctuations is by no means trivial, and it has even been claimed that in confined systems Gaussian fluctuations are valid only over very short distances [28]. Substantial progress has been made recently in modifying the basic RWM to include boundary effects [29–35], supported by numerical evidence [36], and there appears to be no reason to believe that the Gaussian assumption fails in the vicinity of a system’s boundary. Here, we present experimental measurements demonstrating the validity of boundary-adapted RWMs, based on Dirichlet conditions on an infinite straight wall.

The intensity distributions in a two-dimensional chaotic microwave cavity, as shown in Fig. 1, are well understood [23], although the distribution of current critical points has not previously been studied in detail. In addition to the density fluctuations of vortices and saddle points against a Dirichlet boundary, we measure the vortex-vortex correlation function (including the case signed by circulation) and the vortex-saddle and saddle-saddle correlation functions, comparing against predictions of the RWM.

Although some of the theoretical predictions we compare with have been derived before (such as the vortex-vortex correlation functions [25,26] and vortex density fluctuations against a straight wall [29,30]), others are new. In particular, we derive the density fluctuations of saddle points in the presence of an infinite straight boundary on which the wave satisfies mixed (Robin) boundary conditions, and although we were unable to derive exact saddle correlation functions analytically, we have found large- r asymptotic approximations to these functions.

The paper is organized as follows. In Sec. II we explain the experimental setup and techniques used to locate the critical points in the microwave cavity. General definitions

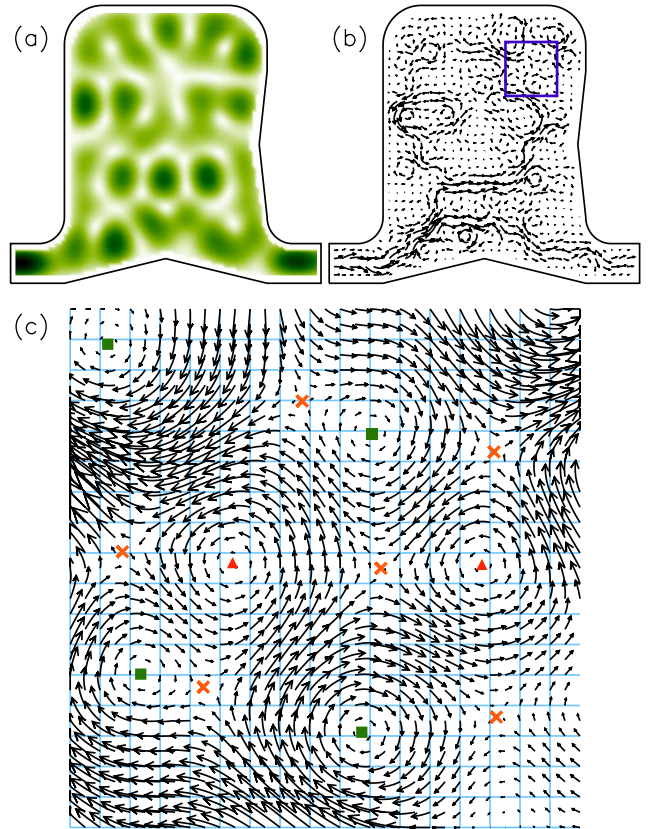


FIG. 1. (Color online) Morphology of typical complex wave function ψ in the open quantum billiard of our experiments: (a) modulus (intensity) $|\psi|^2$, (b) current flow $\text{Im } \psi^* \nabla \psi$, and (c) blowup of (b), demonstrating the critical points we study. Counterclockwise vortices are marked by triangles (red), clockwise ones by squares (green). The saddle points are marked by crosses (orange). Our points of measurement are the crossing points in the background grid.

and properties of critical points of the current associated with the Helmholtz equation, as well as the expressions for densities and correlations, are described in Sec. III. This is followed by Sec. IV, which describes our RWM calculations: the model is introduced in Sec. IV A, and details follow for bulk correlation functions (Sec. IV B) and densities near a straight boundary satisfying Robin conditions (Sec. IV C). The experimental results are compared with the theoretical predictions in Sec. V.

II. EXPERIMENTAL SETUP

We here report on the measurement of correlations functions of saddle and vortex points in an open billiard system including effects of the boundaries. The basic principles of the experiment can be found in Ref. [37]. We used a rounded rectangular cavity ($21 \text{ cm} \times 16 \text{ cm}$) coupled to two waveguides of width 3 cm with a cutoff frequency at $\nu_T = 5 \text{ GHz}$. To break the symmetry and to block direct transport, two triangular obstacles with a length of 12 cm and a height of 1 cm were placed in the resonator. Absorbers were placed at the end of the leads to avoid reflection. We scanned

this billiard on a square grid of 2.5 mm with a movable antenna A_1 and measured transmission S_{12} in the range of 4–18 GHz from a fixed antenna A_2 in the end of the right lead. The fixed antenna had a metallic core of diameter 1 mm and a Teflon coating, while the probe antenna A_1 was a thin wire of diameter 0.2 mm to minimize the leakage current. The lengths of antennas A_1 and A_2 were 4 and 5 mm, respectively.

For microwave frequencies $\nu < c/2d = 18.75$ GHz, where c is the velocity of light and d is the resonator height, the billiard is quasi-two-dimensional. In this regime there is an exact correspondence between electrodynamics and quantum mechanics, where the component of the electric field perpendicular to the plane of the microwave billiard, E_z , corresponds to the quantum-mechanical wave function ψ . Figure 1 shows typical intensity and current patterns thus obtained. Additionally a close-up of the flow pattern is shown to visualize the structure and shows the different types of critical points in the flow. The flow pattern shown in Fig. 1 displays some nonuniformity, but notwithstanding this fact, the distribution of intensities is described perfectly well in terms of the RMW.

We previously have reported results on vortex pair correlation functions and nearest-neighbor distance distributions [38,39] for vortex points. Through improvements in data analysis, we have been able to study the saddle points of the current in addition to the vortices and significantly reduce the effects of noise in our measured correlation functions. These improvements are sketched in the following. We have increased the spatial resolution by a factor of 2 compared to our previous measurements before, and we now use additionally a bilinear interpolation method for the individual components of the flow. Using the bilinear interpolation, we estimate the nodal lines of the individual flow components, enabling us to get the exact position for vortex and saddle points within this approximation. The extraction of critical point locations is now fully automatic, allowing large samples of data to be analyzed. One can see the effect of these improvements in the better results for the pair correlation functions (good agreements also for small kr) and the charge correlation function which we can present here.

For $k\Delta r < 1$, where Δr is the grid length, holding in the whole frequency range studied, the spatial accuracy of the bilinear interpolation amounts to some percent of the grid size. The technique encounters its limits whenever there are three critical points within one grid element at the same time. These events are too rare to spoil the measured distribution and correlation functions.

III. CURRENT CRITICAL-POINT DENSITIES

In this section and following, we assume that the complex wave function $\psi(\vec{r}) = \xi(\vec{r}) + i\eta(\vec{r})$ has no particular symmetries or properties, beyond satisfying Eq. (1). The current \vec{j} , from Eq. (2), can therefore be written

$$\vec{j} = (\xi\eta_x - \eta\xi_x, \xi\eta_y - \eta\xi_y), \quad (3)$$

where here and hereafter, subscripts after scalars denote partial derivatives—e.g., $\eta_x = \partial_x \eta$. The current is zero at vortices,

where $\psi = \xi = \eta = 0$, and at saddle points, where $\xi/\eta = \xi_x/\eta_x = \xi_y/\eta_y$ (if $\eta = 0$, there is equality between the reciprocals of these terms).

The quantity which distinguishes vortices from saddles is the Jacobian

$$\mathcal{J} = \partial_x j_x \partial_y j_y - \partial_y j_x \partial_x j_y, \quad (4)$$

which is positive at vortices and negative at saddles. Since ψ satisfies Eq. (1), \mathcal{J} separates into two contributions [27]:

$$\mathcal{J} = \mathcal{J}_v - \mathcal{J}_s, \quad (5)$$

where

$$\mathcal{J}_v \equiv (\xi_x \eta_y - \xi_y \eta_x)^2, \quad (6)$$

$$\mathcal{J}_s \equiv \frac{1}{2}(\xi\eta_{xx} - \eta\xi_{xx})^2 + \frac{1}{2}(\xi\eta_{yy} - \eta\xi_{yy})^2 + (\xi\eta_{xy} - \eta\xi_{xy})^2. \quad (7)$$

Obviously, $\mathcal{J}_v = 0$ at saddle points and $\mathcal{J}_s = 0$ at vortices. This fact, combined with positive-definiteness of the two parts of the Jacobian, implies that $|\mathcal{J}| = \mathcal{J}_v$ at vortices and $|\mathcal{J}| = \mathcal{J}_s$ at saddle points.

These quantities can be used to define functions which find critical points (vortices or saddles) at position \vec{r} . The density of critical points, with a unit δ function at each zero point of \vec{j} , is given by

$$D_{\text{crit}}(\vec{r}) \equiv \sum_{\{\vec{r}; \vec{j}(\vec{r})=0\}} \delta^2(\vec{r}) = \delta^2(\vec{j}(\vec{r})) |\mathcal{J}(\vec{r})|. \quad (8)$$

By the separation of \mathcal{J} above, this gives the saddle density [27]

$$D_s(\vec{r}) \equiv \delta^2(\vec{j}(\vec{r})) \mathcal{J}_s(\vec{r}) \quad (9)$$

and the vortex density [25–27]

$$D_v(\vec{r}) \equiv \delta^2(\vec{j}(\vec{r})) \mathcal{J}_v(\vec{r}) = \delta(\xi)\delta(\eta) |\xi_x \eta_y - \xi_y \eta_x|. \quad (10)$$

The vortex sign (sense of circulation) is given by

$$S \equiv \text{sgn}(\xi_x \eta_y - \xi_y \eta_x), \quad (11)$$

so removing modulus signs gives the signed vortex density.

The number and location of critical points for a given field must be found by explicitly solving the set of equations $\vec{j}(\vec{r}) = 0$. This of course requires precise knowledge of the spatial dependence of the particular solution $\psi(\vec{r})$ in which we are interested. The task of solving the Helmholtz equation in cases where the geometry of the confinement (transversal section of the waveguide) is such that Eq. (1) is not separable is usually very demanding. This makes the function-by-function study of current morphology almost impossible.

A suitable way to overcome this complication is to use a statistical approach. This idea is based on the strong uniformity of the solutions of the Helmholtz equation with nonintegrable geometries (see, for example, Fig. 1), indicating that their main properties actually depend on far fewer parameters than the full solution itself. We therefore consider, instead of a given set of solutions of the Helmholtz equation,

an *ensemble* of fields. This ensemble will be constructed in such a way that the most general and basic properties of the exact solutions are respected, in the hope that these general properties suffice to fix the morphology fluctuations. The ensemble we choose is the usual RWM discussed in the Introduction or the boundary-adapted model of Refs. [29,30].

Delaying on giving the appropriate definition of the RWM until the next section, we merely write the average over the ensemble $\langle \dots \rangle$. In this paper, we compare theoretical RWM predictions and experimental measurements of the average density fluctuations

$$\rho_\alpha(\vec{r}) = \frac{4\pi}{k^2} \langle D_\alpha(\vec{r}) \rangle \quad (12)$$

and two-point correlations

$$g_{\alpha\beta}(\vec{r}_2, \vec{r}_1) = \left(\frac{4\pi}{k^2} \right)^2 \langle D_\alpha(\vec{r}_2) D_\beta(\vec{r}_1) \rangle, \quad (13)$$

where α, β are v, s. These expressions have been normalized against the bulk average vortex density (and saddle density) $k^2/4\pi$ [25–27]. Statistical symmetries in the RWMs will mean that the densities ρ and correlations g have simpler functional dependence. Two-point correlation functions can also be considered which take topological signs into account, such as the vortex topological charge correlation function

$$g_Q(\vec{r}_1, \vec{r}_2) = \frac{\langle D_v(\vec{r}_1) \mathcal{S}(\vec{r}_1) D_v(\vec{r}_2) \mathcal{S}(\vec{r}_2) \rangle}{(k^2/4\pi)^2}, \quad (14)$$

where the effect of the signum \mathcal{S} functions of Eq. (11) is to negate the modulus signs in D_v ; the vortices are signed by their sense of circulation. Current critical-point correlation functions can be written down in terms of the correlation functions $g_{\alpha\beta}$. If the two-point critical-point correlation function is denoted g_{crit} and g_I the function signed by the Poincaré index (positive for vortices, negative for saddles), we have

$$g_{\text{crit}}(\vec{r}_1, \vec{r}_2) = \frac{1}{4} [g_{\text{vv}}(\vec{r}_1, \vec{r}_2) + g_{\text{ss}}(\vec{r}_1, \vec{r}_2) + 2g_{\text{vs}}(\vec{r}_1, \vec{r}_2)], \quad (15)$$

$$g_I(\vec{r}_1, \vec{r}_2) = \frac{1}{4} [g_{\text{vv}}(\vec{r}_1, \vec{r}_2) + g_{\text{ss}}(\vec{r}_1, \vec{r}_2) - 2g_{\text{vs}}(\vec{r}_1, \vec{r}_2)]. \quad (16)$$

IV. AVERAGE DENSITIES AND CORRELATIONS OF CRITICAL POINTS WITHIN THE RANDOM WAVE MODEL

A. RWM: Basic definition and field correlations

Wave functions in cavities with nonintegrable geometries have two independent and remarkable properties, both thoroughly checked numerically and experimentally. First, their spatial fluctuations are very well described by Gaussian statistics and, second, the spatial two-point correlation function (which uniquely characterizes any Gaussian distribution) is independent of the particular geometry, being a universal

function of the position and energy. These two properties are strictly satisfied if one assumes that the wave field, satisfying the Helmholtz equation (1), is a superposition of infinitely many complex plane waves with equal wave number k and uniformly random directions and phases. Explicitly, this is the limit as $N \rightarrow \infty$ of the random superpositions

$$\psi_{\text{RWM}}(x, y) = \sqrt{\frac{2}{N}} \sum_{n=1}^N \exp[ik(x \cos \theta_n + y \sin \theta_n) + i\chi_n], \quad (17)$$

where θ_n and χ_n are independent and uniformly distributed between 0 and 2π . ψ_{RWM} is normalized so $\langle \xi^2 \rangle = \langle \eta^2 \rangle = 1$. The real and imaginary parts are statistically independent. These assumptions are appropriate to our experimental open billiards [16]. The RWM is ergodic in the bulk—spatial averages are equivalent to ensemble averages. We will describe the boundary-adapted random wave model at the end of this subsection.

The central-limit theorem ensures that, in the limit of infinitely many superposed plane waves, the probability density function of the value of the wave at each point has a complex circular Gaussian distribution [7,25]. Furthermore, all derivatives of the field are also Gaussian random variables, which may have nonvanishing correlations with each other and the original field.

The assumption that the field and its derivatives possess multivariate Gaussian statistics implies that, for a functional $\mathcal{F}[\vec{u}]$, depending on the field and its derivatives at possibly different points, we have

$$\langle \mathcal{F} \rangle = \frac{1}{\sqrt{(2\pi)^n \det \mathbf{M}}} \int_{-\infty}^{\infty} \mathcal{F}[\vec{u}] e^{-(1/2)\vec{u} \cdot \mathbf{M}^{-1} \cdot \vec{u}} d^n \vec{u}, \quad (18)$$

where \vec{u} is an n -dimensional vector consisting of the relevant Gaussian random fields $\xi(\vec{r}_1)$, $\partial_y \eta(\vec{r}_2)$, etc., appearing in \mathcal{F} , and \mathbf{M} is the $n \times n$ matrix of correlations with entries M_{ij} :

$$M_{ij} = \langle u_i u_j \rangle. \quad (19)$$

Calculating the densities of morphological features in the RWM is therefore reduced to a Gaussian integral, whose difficulty depends on the complexity of the functional \mathcal{F} . For instance, the average density of vortices or saddles in the bulk isotropic random waves can be calculated with $\mathcal{F} = D_v$ or D_s from Eqs. (9) and (10); as discussed previously, these are known to be equal constants, with value $k^2/4\pi$ [27]. In this paper, we concentrate on two specific types of functionals \mathcal{F} .

In Sec. IV B, we consider two-point correlations $g_{\alpha\beta}$ in the bulk isotropic random wave model, where \mathcal{F} is given by $D_\alpha(\vec{r}_1) D_\beta(\vec{r}_2)$, with $\alpha, \beta = v, s$. These expressions are the average densities of vortices or saddles at two points, depending only on the scaled distance

$$R \equiv k|\vec{r}_2 - \vec{r}_1|, \quad (20)$$

by isotropy. These critical point correlation functions depend

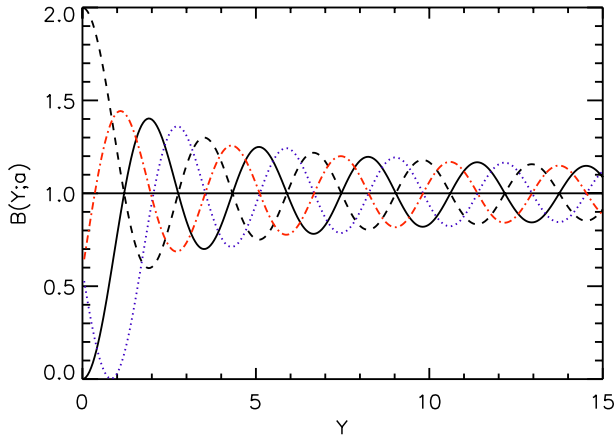


FIG. 2. (Color online) The normalized mean field intensity $B(Y; a)$, plotted against Y for various choices of Robin parameter a : $a=0$ —i.e., Dirichlet conditions (solid, black line); $a=\pi/4$ (dotted, blue line); $a=\pi/2$ —i.e., Neumann conditions (dashed, black line); $a=-\pi/4$ (dashed-dotted, red line). The horizontal black line at $B(Y; a)=1$ corresponds to the asymptotic limit for $Y \rightarrow \infty$.

only on the two-point field correlation function, given by

$$C(R) = \frac{1}{2} \langle \psi(\vec{r}_1) \psi^*(\vec{r}_2) \rangle = \langle \xi(\vec{r}_1) \xi(\vec{r}_2) \rangle = \langle \eta(\vec{r}_1) \eta(\vec{r}_2) \rangle. \quad (21)$$

All two-point correlation functions of derivatives of the field can be expressed in terms of derivatives of $C(R)$. It is well known [9] that the field correlation function of the two-dimensional isotropic RWM is given by the Bessel function

$$C(R) = J_0(R). \quad (22)$$

Much of our argument will be based on asymptotic approximations for large R , in which, to leading order,

$$C(R) \sim \sqrt{\frac{2}{\pi R}} \cos(R - \pi/4). \quad (23)$$

The second type of functional we consider is based on the vortex and saddle densities D_v and D_s in the so-called boundary-adapted (RWM). In this model, the wave with $y \geq 0$ is assumed to satisfy a homogeneous boundary condition along the infinite straight line $y=0$. As above, we will use dimensionless Cartesian coordinates

$$X \equiv kx, \quad Y \equiv ky. \quad (24)$$

Although our experimental data are for Dirichlet conditions only [$\psi(X, 0)=0$], our discussion will be framed in terms of the most general boundary conditions: namely, mixed (Robin) conditions

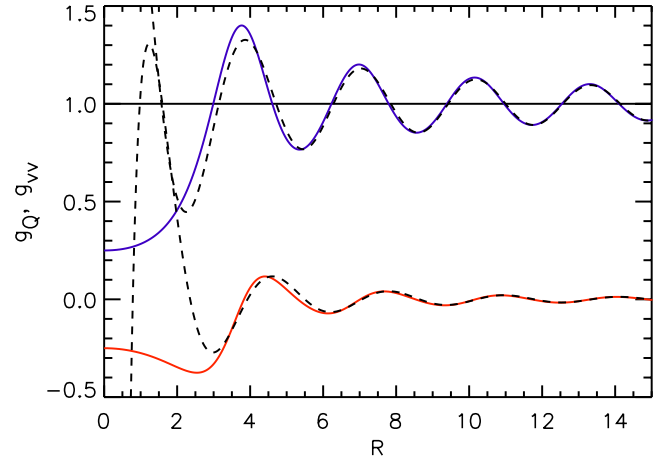


FIG. 3. (Color online) Analytic two-point correlation functions $g_{vv}(R)$ (blue line, top) and $g_Q(R)$ (red line, bottom), plotted against R . The black line is the asymptotic value of 1 for $g_{vv}(R)$ as $R \rightarrow \infty$. The analytic functions compare well with their asymptotic approximations (dashed line) for $R \geq 4$.

$$\psi(X, 0) \cos a + \partial_y \psi(X, 0) \sin a = 0, \quad (25)$$

where a is a constant with $0 \leq a < \pi$. Dirichlet conditions correspond to $a=0$ and Neumann to $a=\pi/2$.

Berry and Ishio [30] constructed a natural RWM satisfying Eq. (25). It is similar in form to the RWM of Eq. (17), although has a weighting factor on each random wave:

$$\begin{aligned} \psi_{\text{RWM}}(X, Y; a) = & \sqrt{\frac{2}{N}} \sum_{n=1}^N \exp(iX \cos \theta_n + i\chi_n) \\ & \times \frac{\sin(Y \sin \theta_n) - \tau \sin \theta_n \cos(Y \sin \theta_n)}{\sqrt{1 + \tau^2 \sin^2 \theta_n}}, \end{aligned} \quad (26)$$

with $\tau = \tan a$ [cf. Ref. [30], Eq. (2)]. This was used to calculate the vortex density as a function of distance Y from the boundary, and general a , generalizing previous work [29] for Dirichlet and Neumann conditions. We will calculate the corresponding Y -dependent saddle-point density in Sec. IV C. The critical-point density calculations depend on the Y -dependent, one-point quadratic field correlation

$$B(Y; a) \equiv \langle \xi(X, Y)^2 \rangle = \langle \eta(X, Y)^2 \rangle. \quad (27)$$

For general a , the function $B(Y; a)$ for the mixed-boundary-condition RWM of Ref. [30] cannot be expressed in terms of elementary functions, although it has a straightforward integral representation

$$B(Y; a) = 1 - \frac{2}{\pi} \int_0^{\pi/2} d\theta \frac{(1 - \tau^2 \sin^2 \theta) \cos(2Y \sin \theta) + 2\tau \sin \theta \sin(2Y \sin \theta)}{1 + \tau^2 \sin^2 \theta}. \quad (28)$$

For Dirichlet and Neumann conditions, B can be expressed in terms of the Bessel function J_0 :

$$B\left(Y; \frac{0}{\pi/2}\right) = 1 \mp J_0(2Y). \quad (29)$$

It is straightforward to find an asymptotic approximation for $B(Y; a)$,

$$B(Y; a) \sim 1 - \frac{1}{\sqrt{\pi Y}} \cos(2Y - 2a - \pi/4), \quad (30)$$

consistent with Eq. (29). The field intensity fluctuation $B(Y; a)$ is plotted as a function of Y for various choices of a in Fig. 2. Equation (30) may also be found from the semiclassical approximation for the two-point correlation function in the presence of Robin boundaries. In this case, a enters through the semiclassical phase [35].

B. Spatial correlations of current vortices and saddles: Bulk results

Correlations of vortices and related objects have been the subject of much study in the isotropic RWM. In particular, the signed vortex-vortex correlation function $g_Q(R)$, defined in Eq. (14), is known to have a remarkably simple form [25,40–45]

$$g_Q(R) = \frac{4}{R} \frac{d}{dR} \left[\frac{d \arcsin[J_0(R)]}{dR} \right]^2. \quad (31)$$

This equation (with J_0 replaced by a suitable two-point function) holds for general isotropic Gaussian random fields, not just the random solutions of the Helmholtz equation studied here. On account of the isotropy of the distribution in the phase of the field ψ , g_Q satisfies the “topological charge screening relation” (ignoring the self-interaction at $R=0$) [25,40–45]

$$\frac{1}{2} \int_0^\infty dR R g_Q(R) = -1. \quad (32)$$

For $R \gg 1$, $g_Q(R) \sim 8 \cos(2R) / \pi R^2$. The oscillation period of $g_Q(R)$ is twice that of the correlation function $C(R)$ since there are two nodes per oscillation of J_0 .

However, unsigned correlation functions, such as those involving saddle points, do not have such a simple form. The vortex-vortex correlation function $g_{vv}(R)$ was found exactly as a complicated single integral in Refs. [25,26] and is given here for completeness in Appendix A. It is also written down in Ref. [46], Eqs. (32)–(35) (also see Ref. [47], p. 83), in a very complicated expression involving various elliptic integrals. Using similar techniques involving computer algebra, our attempts to extract $g_{vs}(R)$ and $g_{ss}(R)$ analytically were unsuccessful.

Instead of exact forms, we therefore found asymptotic expressions for these correlation functions. To do this, we developed a scheme based on an asymptotic expansion of the correlation matrix through the asymptotic expansion of the Bessel function. This scheme was also used to find an asymptotic expression for $g_{vv}(R)$. The details of this scheme are given in Appendix B. Our asymptotic argument is similar to the asymptotic two-point correlation function derived for gradient saddles the real RWM [48], based on functional differentiation.

The asymptotic expansion is in inverse powers of \sqrt{R} and clearly fails for small R (comparison with the experimental results suggests that the approximation is good for $R \gtrsim 3$). Explicitly, the relevant asymptotic approximations to order $O(R^{-1})$ of the RWM vortex-vortex, vortex-saddle, and saddle-saddle pair correlations are

$$g_{vv}(R) \sim 1 + \frac{4 \sin 2R}{\pi R}, \quad (33)$$

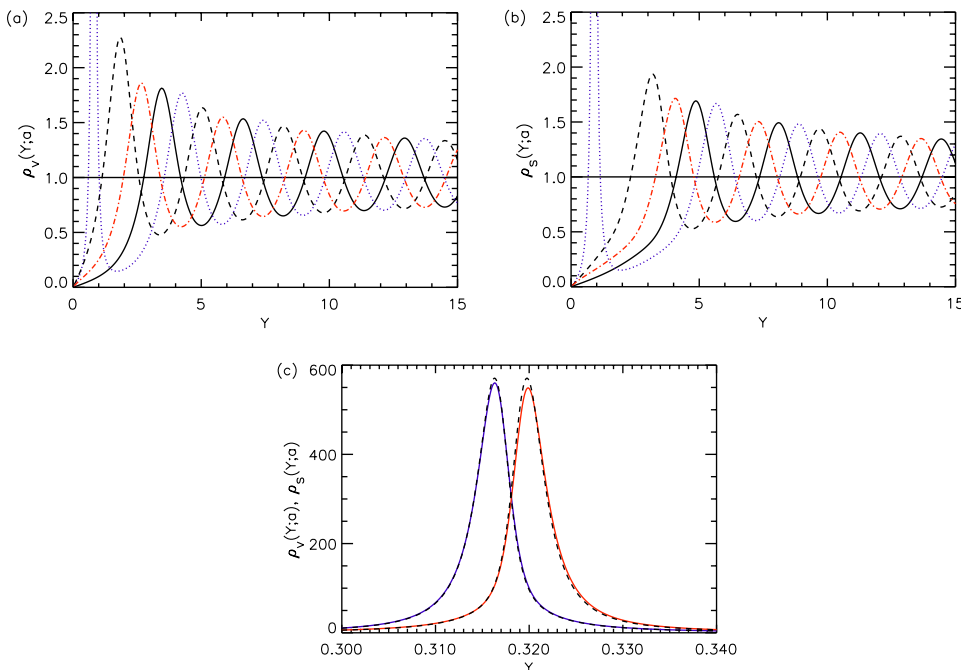


FIG. 4. (Color online) Density oscillations of critical points as a function of distance Y from a straight wall satisfying mixed Robin conditions: (a) $\rho_v(Y; a)$ and (b) $\rho_s(Y; a)$. Line styles and colors represent the same choices of a as in Fig. 2; the black line is at 1 (the asymptotic limit for $Y \rightarrow \infty$); the two densities are clearly out of phase for $Y \gtrsim 4$. (c) Peak in the densities for $a = \pi/10$: ρ_v (left peak, blue line) and ρ_s (right peak, red line). The dashed lines correspond to the small- a forms, as in Eqs. (42) and (43).

$$g_{vs}(R) \sim 1 - \frac{4 \sin 2R}{\pi R}, \quad (34)$$

$$g_{ss}(R) \sim 1 + \frac{4 \sin 2R}{\pi R}. \quad (35)$$

Figure 3 is a plot of $g_{vv}(R)$, computed analytically [46] and from the asymptotic form (33). The two-point correlation functions for vortices of the same sign, $g_{++}(R)=g_{--}(R) \equiv \frac{1}{2}[g_{vv}(R)+g_Q(R)]$, and opposite sign, $g_{+-}(R) \equiv \frac{1}{2}[g_{vv}(R)-g_Q(R)]$ oscillate in phase [21] since $g_Q \sim O(R^{-2})$ decays more swiftly than $g_{vv}(R)$. These equations demonstrate that critical points—that is, vortices (whose Poincaré index is +1) and saddles (with index -1)—oscillate out of phase.

Equations (33)–(35) can be used to estimate asymptotically the critical-point two-point functions $g_{\text{crit}}(R)$ and its Poincaré index-signed analog $g_f(R)$, defined in Eqs. (15) and (16):

$$g_{\text{crit}}(R) \sim 1 + O(R^{-2}), \quad (36)$$

$$g_f(R) \sim 4 \sin(2R)/\pi R. \quad (37)$$

$g_f(R)$ decays rather slowly, in contrast to the long-range correlations of topological charges of other RWMs, such as critical points of the gradient in the real RWM [43,44], which decay to leading order like $O(R^{-3})$. It would therefore be interesting to establish whether the Poincaré index satis-

fies a screening relation analogous to Eq. (32), since convergence in the integral is marginal.

C. Densities of critical points near mixed boundaries

In the boundary-adapted RWM of Eq. (26), the density of vortices and saddles oscillates with distance Y from the boundary. The form of the vortex and saddle density functions depends only on the function $B(Y;a)$ of Eq. (27); the result of the actual Gaussian integral is independent of the value of parameter a . The entries of the correlation matrix, of course, do depend on a , and all may be written as linear combinations of $B(Y;a)$ and its derivatives with respect to Y .

The mean vortex density in the boundary-adapted RWM is [29]

$$\rho_v(Y;a) = \frac{\sqrt{4B+B''} - 1\sqrt{B(2+B'')-B'^2}}{2B^{3/2}}, \quad (38)$$

where the dependence of B on Y and a is suppressed and the prime denotes the partial derivative with respect to Y . The density is normalized with respect to the bulk density, so $\lim_{Y \rightarrow \infty} \rho_v(Y;a) = 1$. This equation is the same as Ref. [29], Eq. (40).

Since the saddle density $D_s(\vec{r})$ of Eq. (9) does not involve modulus signs, the calculation of the average saddle density in the boundary-adapted RWM uses straightforward Gaussian integration techniques, as outlined in Appendix C. The resulting density is

$$\begin{aligned} \rho_s(Y;a) = & \frac{B^{1/2}}{(4B+B''-2)^{3/2}(B(2+B'')-B'^2)^{3/2}} (16-64B+64B^2+16B'^2-64BB'^2+16B'^4-16B''+64B^2B''-32BB'^2B'' \\ & +16BB''^2+16B^2B''^2-4B'^2B''^2+4B''^3-B''^4+8B'B'''-32BB'B''' +8B'^3B'''-8B'B''B''' +2B'B''^2B'''-4B^2B''^2 \\ & +B'^2B''^2-2BB''B''^2-8BB''''+16B^2B''''+4B'^2B''''-8BB'^2B''''+8B^2B''B''''-2B'^2B''B''''+2BB''^2B''''). \end{aligned} \quad (39)$$

Asymptotically, for $Y \gg 1$ we find

$$\rho_v(Y;a) \sim 1 + \frac{2 \cos \left[2(Y-a) - \frac{\pi}{4} \right]}{\sqrt{\pi Y}} + \frac{1 + 5 \sin[4(Y-a)]}{4\pi Y}, \quad (40)$$

$$\rho_s(Y;a) \sim 1 - \frac{2 \cos \left[2(Y-a) - \frac{\pi}{4} \right]}{\sqrt{\pi Y}} + \frac{1 + 5 \sin[4(Y-a)]}{4\pi Y}. \quad (41)$$

[Equation (40) was demonstrated in Ref. [30].] Therefore the leading-order oscillations in vortex and saddle densities are exactly out of phase, as in the two-point correlation functions discussed in the previous subsection. Also, as with the correlation functions, the oscillations have twice the periodicity of the underlying correlation function (again, as nodes occur

with double the frequency of a sinusoidal wave). The mean saddle density for several choices of a is plotted in Fig. 4.

As shown in Ref. [30], when $a \ll 1$, there is a large additional peak in the vortex density for small R . Robin boundary conditions in this regime are known to have unusual properties, such as admitting negative-energy solutions [49] and diverging momenta on the boundary [50]. When a is small, the peak occurs in the neighborhood $Y \approx a + \varepsilon a^3$, where $\rho_v(Y;a)$ has the skewed-Lorentzian form [30]

$$\rho_v(Y = a + a^3 \varepsilon; a) \approx \frac{12\sqrt{1+4(6\varepsilon-1)^2}}{a^3[1+(12\varepsilon-1)^2]^{3/2}}, \quad (42)$$

with a peak near $Y = a + a^3/12$ of height approximately $24\sqrt{2}/a^3$. Analysis of Eq. (39) reveals that the saddles, too, have a peak for small a , and an analogous argument as for vortices gives, for $a \ll 1$,

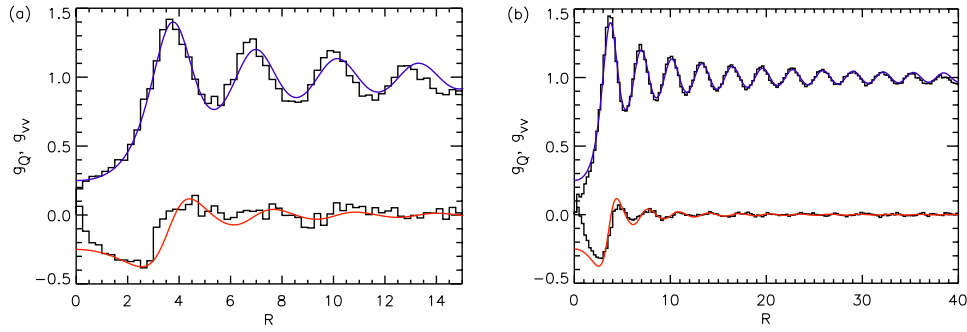


FIG. 5. (Color online) Experimental vortex pair correlation $g_{vv}(R)$ (top histogram) and charge correlation function $g_Q(R)$ (bottom histogram) in (a) the low-frequency regime ($5 \text{ GHz} < \nu < 9 \text{ GHz}$) and (b) the higher-frequency regime ($15 \text{ GHz} < \nu < 18.6 \text{ GHz}$). The solid lines correspond to the analytic prediction of the RWM discussed in Sec. IV B, using the exact formula for $g_{vv}(R)$ rather than the asymptotic form.

$$\rho_s(Y = a + a^3 \varepsilon; a) \approx \frac{12\sqrt{2 + 24\varepsilon(6\varepsilon - 1)}}{a^3[1 + 4(6\varepsilon - 1)^2]^{3/2}}, \quad (43)$$

that is, a peak of almost the same shape and magnitude as for vortices, but with a maximum near $Y = a + a^3/6$. This peak ensures that small a does not give rise to an accumulation of total Poincaré index near the boundary. Plots of the $\rho_v(Y; a)$ and $\rho_s(Y; a)$ for $a = \pi/10$ are Fig. 4(c), along with the corresponding approximations.

V. COMPARISON BETWEEN EXPERIMENT AND RWM PREDICTIONS

In this section we compare the results of our microwave billiard experiment, outlined in Sec. II with the theoretical predictions of the isotropic and boundary-adapted RWMs described in Sec. IV. Since the distances R and Y are scaled with respect to k as in Eqs. (20) and (24) the experimental results for different frequencies ν have been superimposed, improving the statistics.

Figure 5 shows the comparison between experiment and theory for the vortex-vortex pair correlation functions, both signed [Eq. (31)] and unsigned [Ref. [46], Eqs. (32)–(35)], in two different frequency regimes. Because of the limited resolution due to the measurement grid in the low-frequency regime, the correlation function could only be determined reliably for small kr ; see Fig. 5(a). But in this regime the system size is comparable to the vortex spacing, leading to an influence of the boundary on the measured correlation function and restricting the observable R range up to R_{\max}

$= kL \approx 15$, where L corresponds to a typical length of the system. Due to the boundary effects, the oscillation period of the experimental results is shorter than the theoretical one for the bulk statistics [51–53]. The results for the higher-frequency regime, on the other hand, shown in Fig. 5(b), agrees perfectly with theory for large R , but fails for small R because of the mentioned limited resolution in the measurement. Experimental results for the vortex pair correlation function have been published already previously, though with a by far poorer statistics [39]. All other quantities shown in this section have not been published previously.

Results for the saddle pair correlation function $g_{ss}(R)$ and the vortex-saddle function $g_{vs}(R)$ are plotted in Figs. 6(a) and 6(b) and 6, respectively, with experimental data plotted against the asymptotic formulas (35) and (34). As with the vortex correlation functions, the agreement between theory and experiment is very good for a wide range of R ; since the theoretical formulas are asymptotic, we do not have a theory to compare with the data for small R .

Experimental measurements of the average vortex and saddle density fluctuations against a straight boundary satisfying Dirichlet conditions are shown in Fig. 7, vortex fluctuations in Fig. 7(a) [with theoretical density from Eq. (38)], saddle fluctuations [with theoretical plot from Eq. (39)] in Fig. 7(b). The data have been taken from rectangular windows placed parallel to the left and to the upper straight boundary: see Fig. 1. In the theoretical model, on the other hand, an infinite half-plane has been assumed, thereby neglecting the influence of all the other nearby walls. This probably is the cause for the small deviations between experiment and theory exhibited in Fig. 7.

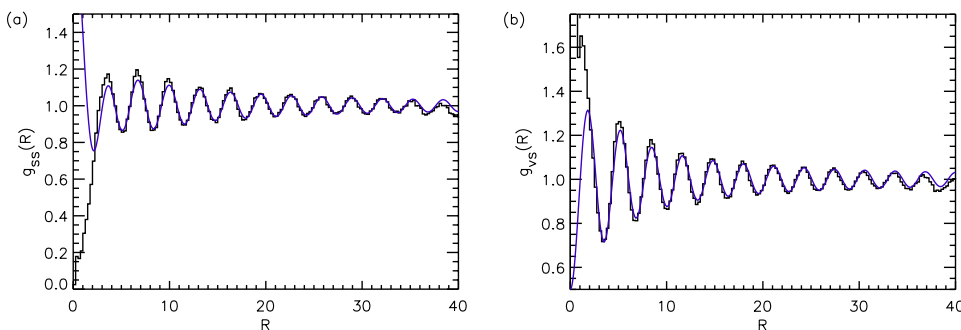


FIG. 6. (Color online) Pair correlations involving saddle points: (a) saddle-saddle correlation function $g_{ss}(R)$ and (b) vortex-saddle function $g_{vs}(R)$. Experimental results (histogram) are plotted against the asymptotic forms [solid, blue line; see Eqs. (34) and (35)].

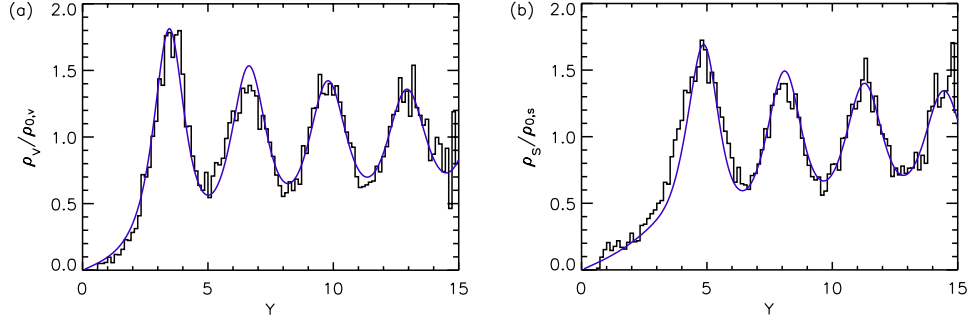


FIG. 7. (Color online) Critical-point density fluctuations as a function of scaled distance Y from a straight wall satisfying Dirichlet boundary conditions: (a) vortex density and (b) saddle density. Experimental results are plotted against the analytic forms for Dirichlet boundary conditions [see Eqs. (38) and (39)].

In summary, by applying a higher grid resolution and a bilinear interpolation technique the flow pattern through an open microwave billiard could be resolved by nearly one order of magnitude better as in previous experiments. This allowed the determination of various distribution and correlation functions for the critical points in the flows, vortices and saddles, which had been inaccessible hitherto.

From the theoretical side, we have presented the universal predictions of the random wave model for the pair correlations of the current's critical points in the bulk and fluctuations in the saddle density dependent on distance from a boundary, showing excellent agreement with the measurements. Although some of the results can be obtained in closed form, an asymptotic method valid for large separations is necessary to construct some important correlations. The leading-order asymptotics of these correlations is sufficient to check topological charge screening, leading to a somewhat surprising behavior of the Poincaré index, which is still to be explained, but is fully supported by the experimental results.

We also contrast the basic assumptions of the boundary-adapted random wave model against experimental results. The influence of the boundary showed up first in an oscillatory behavior in the density of vortices and saddles close to the wall.

ACKNOWLEDGMENTS

This work was funded by the Deutsche Forschungsgemeinschaft via the Forschergruppe 760 ‘‘Scattering Systems with Complex Dynamics.’’ M.R.D. is supported by the Royal Society of London.

APPENDIX A: EXPLICIT FORM OF $g_{vv}(R)$

Here, we give the form for the unsigned vortex-vortex correlation function. It was originally derived in Refs. [25,26] and can most compactly be written as an integral

$$g(R) = \frac{2(1 - J_0^2 - 2J_1^2)}{\pi(1 - J_0^2)^2} \times \int_0^\infty dt \frac{3 - Z + 2Y + (3 + Z - 2Y)t^2 + 2Zt^4}{(1 + t^2)^3 \sqrt{1 + (1 + Z - Y)t^2 + Zt^4}}, \quad (\text{A1})$$

where

$$Y = \frac{16J_1^2(RJ_0^3 - J_1J_0^2 + R(J_1^2 - 1)J_0 + J_1)^2}{R^4(J_0^2 + 2J_1^2 - 1)^2}, \quad (\text{A2})$$

$$Z = \frac{(1 - J_0^2)(R^2 - 4J_1^2)}{R^4[1 - J_0(r)^2 - 2J_1(r)^2]^2} [2(J_0 + 1)J_1 + R(1 - 2J_0^2 - J_0 - 2rJ_1^2)][2J_0J_1 + R(1 - 2J_0^2 - 2J_1^2 - J_2)], \quad (\text{A3})$$

and explicit dependence on R is suppressed from the Bessel functions. With the aid of computer algebra, it is possible to perform the integral in Eq. (A1), giving a rather unwieldy form in terms of elliptic integrals [46].

APPENDIX B: ASYMPTOTIC PAIR CORRELATIONS

In this section we sketch the method we use to calculate the asymptotic (large- R) approximation to the RWM average of an arbitrary functional \mathcal{F} depending on the field and its derivatives at points \vec{r}_1, \vec{r}_2 with $k|\vec{r}_1 - \vec{r}_2| = R$ the scaled distance.

We start with an exact expression for the Gaussian average:

$$\langle \mathcal{F} \rangle = \frac{1}{\sqrt{(2\pi)^{n+m} \det \mathbf{M}}} \int_{-\infty}^{\infty} \mathcal{F}[\vec{u}] e^{-(1/2)\vec{u} \cdot \mathbf{M}^{-1} \cdot \vec{u}} d^{n+m} \vec{u}, \quad (\text{B1})$$

where the vector

$$\vec{u} = (\vec{u}^{(1)}, \vec{u}^{(2)}) \quad (\text{B2})$$

comprises all the relevant degrees of freedom $\vec{u}^{(1)} = (u_1^{(1)}, \dots, u_n^{(1)})$ at position \vec{r}_1 and $\vec{u}^{(2)} = (u_1^{(2)}, \dots, u_m^{(2)})$ at position \vec{r}_2 . With this definition, the correlation matrix has a natural block form

$$\mathbf{M} = \begin{pmatrix} \mathbf{M}^{(1,1)} & \mathbf{M}^{(1,2)} \\ \mathbf{M}^{(2,1)} & \mathbf{M}^{(2,2)} \end{pmatrix}, \quad (\text{B3})$$

where $[\mathbf{M}^{(\alpha,\beta)}]_{i,j} = \langle u_i^{(\alpha)} u_j^{(\beta)} \rangle$. The key step of the method is to observe that the only dependence of the average $\langle \mathcal{F} \rangle$ on the scaled distance R comes from the off-diagonal blocks and the known asymptotic expansion of $\mathbf{M}^{(1,2)}(R)$ will imply an asymptotic expansion of $\langle \mathcal{F} \rangle$. In order to follow this program, we found convenient to switch to the Fourier represen-

tation of the probability distribution in Eq. (B1):

$$\frac{e^{-(1/2)\vec{u}\cdot\mathbf{M}^{-1}\cdot\vec{u}}}{\sqrt{(2\pi)^{n+m}\det\mathbf{M}}} = \int_{-\infty}^{\infty} d^m\vec{w}^{(1)} d^m\vec{w}^{(2)} e^{i(\vec{w}^{(1)},\vec{w}^{(2)}),(\vec{u}^{(1)},\vec{u}^{(2)})} \times e^{-(1/2)(\vec{w}^{(1)},\vec{w}^{(2)})\cdot\mathbf{M}\cdot(\vec{w}^{(1)},\vec{w}^{(2)})}. \quad (\text{B4})$$

Due to the asymptotic form of the off-diagonal block $\mathbf{M}^{(1,2)} \sim 1/\sqrt{R}$, the last line in Eq. (B4) can be written as

$$e^{-(1/2)(\vec{w}^{(1)},\vec{w}^{(2)})\cdot\mathbf{M}\cdot(\vec{w}^{(1)},\vec{w}^{(2)})} = e^{-(1/2)\vec{w}^{(1)}\cdot\mathbf{M}^{(1,1)}\cdot\vec{w}^{(1)}} e^{-(1/2)\vec{w}^{(2)}\cdot\mathbf{M}^{(2,2)}\cdot\vec{w}^{(2)}} \times \left[1 - \vec{w}^{(1)} \cdot \mathbf{M}^{(1,2)} \cdot \vec{w}^{(2)} + \frac{1}{2}(\vec{w}^{(1)} \cdot \mathbf{M}^{(1,2)} \cdot \vec{w}^{(2)})^2 \right] + O(1/R^{3/2}). \quad (\text{B5})$$

We note that, given the particular form of the asymptotic expansion of the Bessel function, the very first term of the asymptotic expansion of the off-diagonal blocks not only gives the leading-order term in $1/\sqrt{R}$ of the average, but also the subleading one of order $1/R$. Beyond the subleading order, higher-order terms of the average require higher-order terms in the expansion of $\mathbf{M}^{(1,2)}$. This has to be considered a very special property of the Bessel-correlated RWM with its characteristic slow ($\sim 1/\sqrt{R}$) decay of correlations.

Substitution of Eq. (B5) into Eq. (B4) results in the asymptotic expansion of the probability distribution, which in turn leads to the sought asymptotic expansion of the average in Eq. (B1). The calculations are simple but tedious, so we merely quote the result. Denoting

$$\mathbf{A} = [\mathbf{M}^{(1)}]^{-1}\mathbf{M}^{(1,2)}[\mathbf{M}^{(2)}]^{-1} \quad (\text{B6})$$

and introducing the tensors

$$F_0 = \langle \mathcal{F} \rangle_0, \quad \mathbf{F}_0^{(\alpha,\beta)} = \langle u_i^{(\alpha)} u_j^{(\beta)} \mathcal{F} \rangle_0, \quad (\text{B7})$$

where $\langle \cdots \rangle_0$ indicates the average in Eq. (B1) with $\mathbf{M}^{(1,2)} = \mathbf{M}^{(2,1)} = 0$, we get finally

$$\begin{aligned} \langle \mathcal{F} \rangle &= F_0 + \text{Tr}\mathbf{A}\mathbf{F}_0^{(2,1)} + \frac{1}{2}F_0\text{Tr}\mathbf{A}\mathbf{M}^{(2,2)}\mathbf{A}^T\mathbf{M}^{(1,1)} \\ &\quad - \frac{1}{2}[\text{Tr}\mathbf{F}_0^{(1,1)}\mathbf{A}\mathbf{M}^{(2,2)}\mathbf{A}^T + \text{Tr}\mathbf{F}_0^{(2,2)}\mathbf{A}^T\mathbf{M}^{(1,1)}\mathbf{A}] \\ &\quad + \frac{1}{2}\text{Tr}\mathbf{A}\mathbf{F}_0^{(2,2)}\mathbf{A}^T\mathbf{F}_0^{(1,1)} + O(1/R^{3/2}). \end{aligned} \quad (\text{B8})$$

Our result, Eq. (B8), allows us to calculate the leading ($\sim 1/\sqrt{R}$) and subleading ($\sim 1/R$) contributions to any correlation in terms of the $\mathbf{M}^{(1,2)} = \mathbf{M}^{(2,1)} = 0$ (uncorrelated) results. It also provides the large- R asymptotics to one-point functionals at points separated a distance $2R$ from an infinite straight boundary.

APPENDIX C: DERIVATION OF THE Y -DEPENDENT SADDLE DENSITY, EQ. (39)

The saddle density at scaled distance Y from a straight boundary can be calculated by standard methods of Gaussian integration (as used, for instance, in Refs. [21,44]), although the details are rather tedious and only outlined here. Normalized by the bulk density, the Y -dependent saddle density is

$$\rho_s(Y) = 4\pi\langle D_Y(Y) \rangle = \frac{1}{\pi} \int d^2\vec{r} \langle \exp(i\vec{j} \cdot \vec{r}) \mathcal{J}_s \rangle. \quad (\text{C1})$$

Since \mathcal{J}_s is a sum of terms, linearity of the average simplifies the Gaussian average to calculations of the form

$$A_{\alpha\beta} = \langle (\xi\eta_{\alpha\beta} - \eta\xi_{\alpha\beta})^2 \exp(i\vec{j} \cdot \vec{r}) \rangle, \quad (\text{C2})$$

where $\alpha\beta = XX, YY$, or XY .

Each $A_{\alpha\beta}$ is an average over an eight-dimensional Gaussian random vector

$$\vec{u} = \{\xi, \xi_X, \xi_Y, \xi_{\alpha\beta}, \eta, \eta_X, \eta_Y, \eta_{\alpha\beta}\}. \quad (\text{C3})$$

The terms in ξ and η are uncorrelated. Denoting either by v and suppressing Y dependence, the relevant nonvanishing correlations follow from Eq. (27), $B = \langle v^2 \rangle$:

$$\langle vv_{YY} \rangle = \frac{1}{2} - \frac{1}{4}B'',$$

$$\langle v_X^2 \rangle = -\frac{1}{2} + B + \frac{1}{4}B'',$$

$$\langle v_Y^2 \rangle = \frac{1}{2} + \frac{1}{4}B'',$$

$$\langle vv_Y \rangle = \frac{1}{2}B',$$

$$\langle v_Y v_{XX} \rangle = -\frac{1}{2}B' - \frac{1}{8}B''',$$

$$\langle v_Y v_{YY} \rangle = \frac{1}{8}B''',$$

$$\langle v_{XX}^2 \rangle = -\frac{5}{8} + B + \frac{1}{2}B'' + \frac{1}{16}B''',$$

$$\langle v_{YY}^2 \rangle = \frac{3}{8} + \frac{1}{16}B''',$$

$$\langle v_{XY}^2 \rangle = \frac{1}{8} + \frac{1}{4}B'' + \frac{1}{16}B''', \quad (\text{C4})$$

where the prime denotes the partial derivative with respect to Y . We denote the appropriate correlation matrix for \vec{u} by $\mathbf{M}_{\vec{u}}$.

The scalar product in the exponent in (C2) can be written as a symmetric quadratic form in \vec{u} :

$$\vec{j} \cdot \vec{i} = \frac{1}{2} \vec{u} \cdot \mathbf{T} \cdot \vec{u}, \quad (\text{C5})$$

where \mathbf{T} depends on t_1 and t_2 .

Therefore, defining the matrix $\Xi \equiv (\mathbf{M}_{\vec{u}}^{-1} + i\mathbf{T})^{-1}$ and $Q \equiv (\xi\eta_{\alpha\beta} - \eta\xi_{\alpha\beta})$, it is straightforward to see

$$\begin{aligned} A_{\alpha\beta} &= \frac{1}{(2\pi)^4 \sqrt{\det \mathbf{M}_{\vec{u}}}} \int d^8 \vec{u} Q^2 \exp\left(-\frac{1}{2} \vec{u} \cdot \Xi^{-1} \cdot \vec{u}\right) \\ &= \sqrt{\frac{\det \Xi}{\det \mathbf{M}_{\vec{u}}}} \left[\Delta^2 \exp\left(-\frac{1}{2} \vec{w} \cdot \Xi \cdot \vec{w}\right) \right]_{\vec{w}=0}, \quad (\text{C6}) \end{aligned}$$

where \vec{w} is a Fourier dual to \vec{u} and Δ is the quadratic form of Fourier derivatives corresponding to Q . The final step in

Gaussian integration by parts reduces to a multilinear combination of entries of Ξ . Each $A_{\alpha\beta}$ can now be integrated with respect to \vec{i} . In terms of the original correlations, the final result is

$$\begin{aligned} \rho_s(Y) &= \frac{\sqrt{B}}{\langle v_X^2 \rangle^{3/2} (B \langle v_Y^2 \rangle - \langle v v_Y \rangle^2)^{3/2}} [(B \langle v_Y^2 \rangle - \langle v v_Y \rangle^2) \langle v_X^2 \rangle \\ &\quad \times (\langle v_{XX}^2 \rangle + \langle v_{YY}^2 \rangle + 2 \langle v_{XY}^2 \rangle) - 2 \langle v_Y v_{XX} \rangle^2 - \langle v_X^2 \rangle \langle v_Y^2 \rangle \\ &\quad \times (\langle v_X^2 \rangle^2 + \langle v v_{YY} \rangle^2) - B \langle v_X^2 \rangle (\langle v_Y v_{XX} \rangle^2 + \langle v_Y v_{YY} \rangle^2) \\ &\quad - 2 \langle v_X^2 \rangle \langle v v_Y \rangle (\langle v_X^2 \rangle \langle v_Y v_{XX} \rangle + \langle v v_{YY} \rangle \langle v_Y v_{YY} \rangle)]. \quad (\text{C7}) \end{aligned}$$

Equation (39) follows from this expression with the appropriate substitutions from Eqs. (C4).

-
- [1] S. O. Rice, Bell Syst. Tech. J. **24**, 46 (1945).
[2] M. S. Longuet-Higgins, Philos. Trans. R. Soc. London, Ser. A **249**, 321 (1957).
[3] M. S. Longuet-Higgins, Philos. Trans. R. Soc. London, Ser. A **250**, 157 (1957).
[4] K. J. Ebeling, in *Physical Acoustics: Principles and Methods*, edited by W. P. Mason and R. N. Thurston (Academic Press, New York, 1984), Vol. 17, p. 233.
[5] G. Tanner and S ndergaard, J. Phys. A **40**, R443 (2007).
[6] U. Frisch, *Turbulence: The Legacy of A. N. Kolmogorov* (Cambridge University Press, Cambridge, England, 1995).
[7] J. W. Goodman, *Speckle Phenomena in Optics: Theory and Applications* (Ben Roberts & Co., Greenwood Village, CO, 2007).
[8] A. R. Liddle and D. H. Lyth, *Cosmological Inflation and Large-Scale Structure* (Cambridge University Press, Cambridge, England, 2000).
[9] M. V. Berry, J. Phys. A **10**, 2083 (1977).
[10] H.-J. St ckmann and J. Stein, Phys. Rev. Lett. **64**, 2215 (1990).
[11] S. Sridhar, Phys. Rev. Lett. **67**, 785 (1991).
[12] H.-D. Gr f, H. L. Harney, H. Lengeler, C. H. Lewenkopf, C. Rangacharyulu, A. Richter, P. Schardt, and H. A. Weidenm ller, Phys. Rev. Lett. **69**, 1296 (1992).
[13] P. So, S. M. Anlage, E. Ott, and R. N. Oerter, Phys. Rev. Lett. **74**, 2662 (1995).
[14] J. Barth lemy, O. Legrand, and F. Mortessagne, Phys. Rev. E **71**, 016205 (2005).
[15] H.-J. St ckmann, *Quantum Chaos—An Introduction* (Cambridge University Press, Cambridge, England, 1999).
[16] U. Kuhl, Eur. Phys. J. Spec. Top. **145**, 103 (2007).
[17] A. D. Mirlin, Phys. Rep. **326**, 259 (2000).
[18] S. Tomsovic, D. Ullmo, and A. B cker, Phys. Rev. Lett. **100**, 164101 (2008).
[19] A. M. Garcia-Garcia, J. D. Urbina, E. A. Yuzbashyan, K. Richter, and B. L. Altshuler, Phys. Rev. Lett. **100**, 187001 (2008).
[20] P. O’Connor, J. Gehlen, and E. J. Heller, Phys. Rev. Lett. **58**, 1296 (1987).
[21] M. R. Dennis, Eur. Phys. J. Spec. Top. **145**, 191 (2007).
[22] P. Šeba, U. Kuhl, M. Barth, and H.-J. St ckmann, J. Phys. A **32**, 8225 (1999).
[23] Y.-H. Kim, U. Kuhl, H.-J. St ckmann, and P. W. Brouwer, Phys. Rev. Lett. **94**, 036804 (2005).
[24] K.-F. Berggren, D. N. Maksimov, A. F. Sadreev, R. H hmann, U. Kuhl, and H.-J. St ckmann, Phys. Rev. E **77**, 066209 (2008).
[25] M. V. Berry and M. R. Dennis, Proc. R. Soc. London, Ser. A **456**, 2059 (2000).
[26] A. I. Saichev, K.-F. Berggren, and A. F. Sadreev, Phys. Rev. E **64**, 036222 (2001).
[27] M. R. Dennis, J. Phys. A **34**, L297 (2001).
[28] I. V. Gornyi and A. D. Mirlin, Phys. Rev. E **65**, 025202(R) (2002).
[29] M. V. Berry, J. Phys. A **35**, 3025 (2002).
[30] M. V. Berry and H. Ishio, J. Phys. A **35**, 5961 (2002).
[31] S. Hortikar and M. Srednicki, Phys. Rev. Lett. **80**, 1646 (1998).
[32] C. T. Wheeler, J. Phys. A **38**, 1491 (2005).
[33] W. E. Bies and E. J. Heller, J. Phys. A **35**, 5673 (2002).
[34] J. D. Urbina and K. Richter, Phys. Rev. Lett. **97**, 214101 (2006).
[35] J. D. Urbina and K. Richter, Phys. Rev. E **70**, 015201(R) (2004).
[36] M. V. Berry and H. Ishio, J. Phys. A **38**, L513 (2005).
[37] U. Kuhl, E. Persson, M. Barth, and H.-J. St ckmann, Eur. Phys. J. B **17**, 253 (2000).
[38] Y.-H. Kim, M. Barth, U. Kuhl, and H.-J. St ckmann, Prog. Theor. Phys. Suppl. **150**, 105 (2003).
[39] M. Barth and H.-J. St ckmann, Phys. Rev. E **65**, 066208 (2002).
[40] B. I. Halperin, in *Physics of Defects*, edited by R. Balian, M. Kl man, and J.-P. Poirier, Les Houches, Session XXXV, 1980, (North-Holland, Amsterdam, 1981), pp. 813–857.
[41] I. Freund and M. Wilkinson, J. Opt. Soc. Am. A **15**, 2892 (1998).
[42] G. Foltin, J. Phys. A **36**, 1729 (2003).
[43] G. Foltin, J. Phys. A **36**, 4561 (2003).
[44] M. R. Dennis, J. Phys. A **36**, 6611 (2003).

- [45] M. Wilkinson, *J. Phys. A* **37**, 6763 (2004).
- [46] M. R. Dennis, *Proc. SPIE* **4403**, 13 (2001).
- [47] M. R. Dennis, Ph.D. thesis, University of Bristol, 2001.
- [48] G. Foltin, e-print arXiv:0302049v1.
- [49] M. Sieber, H. Primack, U. Smilansky, I. Ussishkin, and H. Schanz, *J. Phys. A* **28**, 5041 (1995).
- [50] M. V. Berry and M. R. Dennis, *J. Phys. A* **41**, 135203 (2008).
- [51] A. Bäcker and R. Schubert, *J. Phys. A* **35**, 539 (2002).
- [52] B. Eckhardt, U. Dörr, U. Kuhl, and H.-J. Stöckmann, *Europhys. Lett.* **46**, 134 (1999).
- [53] A. Bäcker and R. Schubert, *J. Phys. A* **32**, 4795 (1999).